Theor Chem Acc (2011) 129:257–270
DOI 10.1007/s00214-011-0932-x

REGULAR ARTICLE

Tuning the electronic structures and optical properties of fluorene-based donor–acceptor copolymers by changing the acceptors: a theoretical study

Yanling Wang · Qiang Peng · Qiufei Hou · Kun Zhao · Ying Liang · Benlin Li

Received: 17 December 2010 / Accepted: 26 March 2011 / Published online: 9 April 2011

Abstract Five fluorene-based conjugated copolymers were studied to explore the effect of acceptor on the electronic and optical properties. Their ground-state, excited-state electronic structures and the tunable optical properties were theoretically investigated using density functional theory (DFT) and time-dependent density functional theory (TDDFT) methods. The acceptors including quinoxaline (**Q**), 2,1,3-benzothiadiazole (**BT**), thieno[3,4-b]pyrazine (**TP**), 2,1,3-benzooxadiazole (**BO**), and pyridopyrazine (**PP**) can significantly influence the copolymers' electronic structures, molecular orbitals, geometric conformations, and optical properties. Calculations were made on systems containing one, two, three, and four oligomers in the neutral, cationic, and anionic structures, which can be extrapolated to infinite chain length polymers. The result indicated that the sequence of the band gap was on the reverse trend of emission wavelength. The strong electron-withdrawing strength of **TP** unit and coplanar backbone in poly[2,7-(9,9′-dihexylfluorene)-*alt*-2,3-dimethyl-5,7-dithien-2-yl-thieno[3,4-b] pyrazine] resulted in the enhanced degree of intramolecular charge transfer (ICT) and lowest band gap. The contribution of acceptors to *IP* was also found to follow the sequence of **TP** < **Q** < **PP** < **BT** < **BO**. The absorption and emission spectra exhibited red-shift with increasing the conjugation lengths. The present study suggested that the electronic and optical properties of donor–acceptor conjugated copolymers were affected by the acceptor structure.

Keywords Donor–acceptor copolymers · Acceptor effect · Absorption · Emission · Density functional theory

Y. Wang · Q. Peng (✉) · Q. Hou · K. Zhao · Y. Liang · B. Li
School of Chemical Engineering and Food Science, Xiangfan University, 441053 Xiangfan, People's Republic of China
e-mail: qiangpengjohnny@yahoo.com

Q. Peng
School of Environmental and Chemical Engineering, Nanchang Hangkong University, 330063 Nanchang, People's Republic of China

1 Introduction

Organic π-conjugated polymers have attracted much scientific and technological research interest because of their potential applications in thin film transistors, nonlinear optical devices, solar cells, and organic light-emitting diodes [1–7]. The band structures of conjugated polymers can be manipulated by the minimization of bond length alternation and incorporation of donor–acceptor systems to tune their electronic and optical properties [8, 9]. On the other hand, the electronic properties of this type of copolymers were found to be greatly affected by intramolecular charge transfer (ICT) [9–12]. Donor–acceptor conjugated copolymers have also been extensively used to achieve low band gaps. Among these copolymers, the electron-donating moieties of fluorene [13–16], thiophene [17–20], and cyclopentadithiophene [16, 21] have been widely reported.

In this work, poly[2,7-(9,9′-dihexylfluorene)-*alt*-2,3-dimethyl-5,7-dithien-2-yl-quinoxaline] (PFDDTQ), poly [2,7-(9,9′-dihexylfluorene)-*alt*-4,7-dithien-2-yl-2,1,3-benzothiadiazole] (PFDTBT), and poly[2,7-(9,9′-dihexylfluorene)-alt-2,3-dimethyl-5,7-dithien-2-yl-thieno[3,4-b]pyrazine] (PFDDTTP) [15] were chosen as target polymers, and another two novel π-conjugated polymers poly [2,7-(9,9′-dihexylfluorene)-*alt*-4,7-dithien-2-yl-2,1,3-benzooxadiazole] (PFDTBO) and poly[2,7-(9,9′-dihexylfluorene)-alt-2,3-dimethyl-5,7-dithien-2-yl-pyridopyrazine] (PFDDTPP) were designed

here, which are structurally similar to PFDTBT and PFDDTQ. These donor–acceptor copolymers based on fluorene and thiophene modified with various electron-withdrawing units of including quinoxaline (**Q**), 2,1,3-benzothiadiazole (**BT**), thieno[3,4-b]pyrazine (**TP**), 2,1,3-benzooxadiazole (**BO**), and pyridopyrazine (**PP**) possessed low band gaps and high hole mobilities, which were desirable for efficient bulk-heterojunction photovoltaic cells. The structures of copolymers are shown in Fig. 1. To rationalize these experimentally observed properties of known polymers [22] and to predict those unknown ones [23], theoretical investigations into the structures and electronic properties of these materials are indispensable. Recently, a series of polymers [24, 25] were studied employing B3LYP/6-31G(d) method.

Here, electronic and optical properties of these conjugated copolymers comprised of alternating fluorene and thiophene derivatives were investigated theoretically by using density functional theory (DFT) and time-dependent density functional theory (TD-DFT) calculations. Different functional groups between two thiophene units are systematically discussed in these fluorene-based copolymers.

2 Computational details

All calculations on the oligomers studied in this work have been made with the Gaussian 09 program [26]. Complete geometry of ground states as well as the cationic and anionic structures of $(FDDTQ)_n$, $(FDTBT)_n$, $(FDDTTP)_n$, and two novel π-conjugated $(FDDTPP)_n$ and $(FDTBO)_n$ ($n = 1$–4) oligomers were optimized by Becke's three parameters hybrid functional (B3LYP) [27–29] with 6-31G(d) basis sets [30], where n refers to the repeated number of monomers. It has been proven that the presence of alkyl groups does not significantly affect the equilibrium geometry, electronic, and optical properties [31]. We use 9,9′-dimethylfluorene to replace 9,9′-dihexylfluorene for the sake of reducing the time of calculation. The related ionization potential (IP), hole extraction potentials (HEP), electron extraction potentials (EEP), energy gap (ΔE) ($\Delta E = E_{LUMO} - E_{HOMO}$), and electron affinity (EA) were obtained by DFT method based on the optimized geometry of the neutral and ionic molecules. All these parameters of $(FDDTQ)_n$, $(FDTBT)_n$, $(FDDTTP)_n$, $(FDDTPP)_n$, and $(FDTBO)_n$ ($n = 1$–4) were obtained through a linear extrapolation technique [32], which had been successfully employed to investigate polymers [33–35]. The absorptions and emissions of these oligomers had also been investigated by TD-DFT [36] method with 6-31G(d) basis set.

3 Results and discussion

3.1 Optimized geometry

The main optimized geometry parameters of $(FDDTQ)_n$, $(FDTBT)_n$, $(FDDTTP)_n$, $(FDDTPP)_n$, and $(FDTBO)_n$ ($n = 1$–4) are shown in Fig. 2 and Table 1. The maximum and averaged changes in the length of these bonds (Δd_{max} and Δd_{av}, respectively) and total changes in the bond

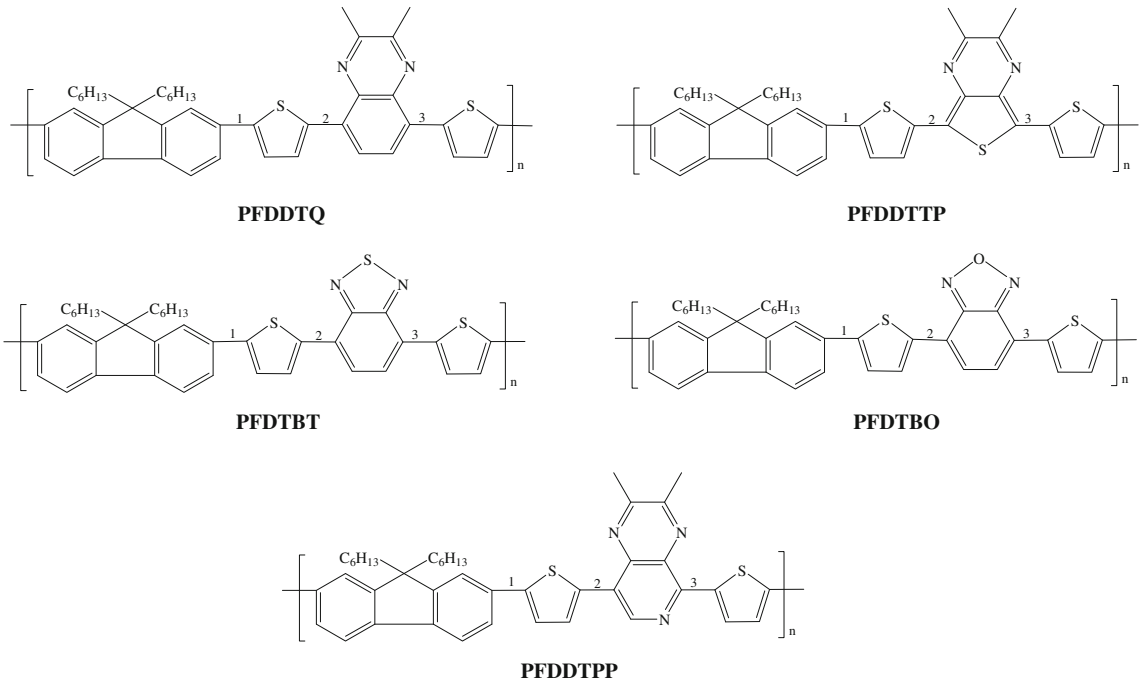

Fig. 1 The structures of the five fluorene-based copolymers

lengths ($\Sigma\Delta d_i$) are summarized in Table 2. Oligomers and polymers were always considered as anti conformation in quantum-chemical calculations [37, 38]. The *syn* and *anti* conformation of $(FDDTQ)_n$, $(FDTBT)_n$, $(FDDTTP)_n$, $(FDDTPP)_n$, and $(FDTBO)_n$ were checked using dimers. As a result, the *anti* conformation is more stable in dimers. So we choose the energetically favorable trans-configuration in the following calculations.

As shown in Fig. 2 and Table 1, the results of the optimized structures for all five copolymers show that the bond lengths and bond angles do not suffer appreciable variation with the oligomer size, which indicates that describing the basic structures of the copolymers as their oligomers is appropriate. As listed in Table 1, the calculated dihedral angles are not 0.0°, which indicate that each oligomer is not linear, but of a screw-type structure. For this reason, this kind of arrangement can minimize the steric effect and stabilize the molecules at the largest extent.

As listed in Table 2, the larger changes in the lengths of the C–C bonds along the molecular backbone from the neutral state to the radical cation/anion state result in the shortest oligomers with increasing the values of n. It is obvious that the bond lengths of $(FDDTTP)_n$ exist the largest change from the ground state to the radical cation/anion state. This is attributed to the unfavorable steric interactions produced by the **TP** units, which increase the rigidity of $(FDDTTP)_n$ oligomer. In above five systems, the values of $\Sigma\Delta d_i$ from the ground state to radical cation state increase from $n = 1$ to 4. These effects are similar to those reported for the oligomers of poly(3,4 -ethylenedioxythiophene) [39] at the same theoretical level.

3.2 Frontier molecular orbitals

To shed light on the chemical activity of these donor–acceptor conjugated copolymers, energies of the frontier orbital of the five oligomers are listed in Table 3. The corresponding contour plots of these orbitals are illustrated in Fig. 3.

As shown in Fig. 3, there is inter-ring antibonding between the bridge atoms, and there is intra-ring bonding between the bridge carbon atom and its neighbor in the HOMO. On the contrary, there is inter-ring bonding in the bridge single bond and intra-ring antibonding between the bridge atom and its conjoined atoms in the LUMO. In general, the HOMO possesses antibonding character between the subunits. However, the LUMO generally shows a bonding character between the subunits. The HOMOs of $(FDDTQ)_2$, $(FDTBT)_2$, $(FDDTTP)_2$, $(FDDTPP)_2$, and $(FDTBO)_2$ are quite delocalized the whole π-conjugated backbone with similar character, while the LUMOs are localized on the donor and acceptor units. For tetramer, the localization of the electronic cloud distributing in the middle part of the polymer

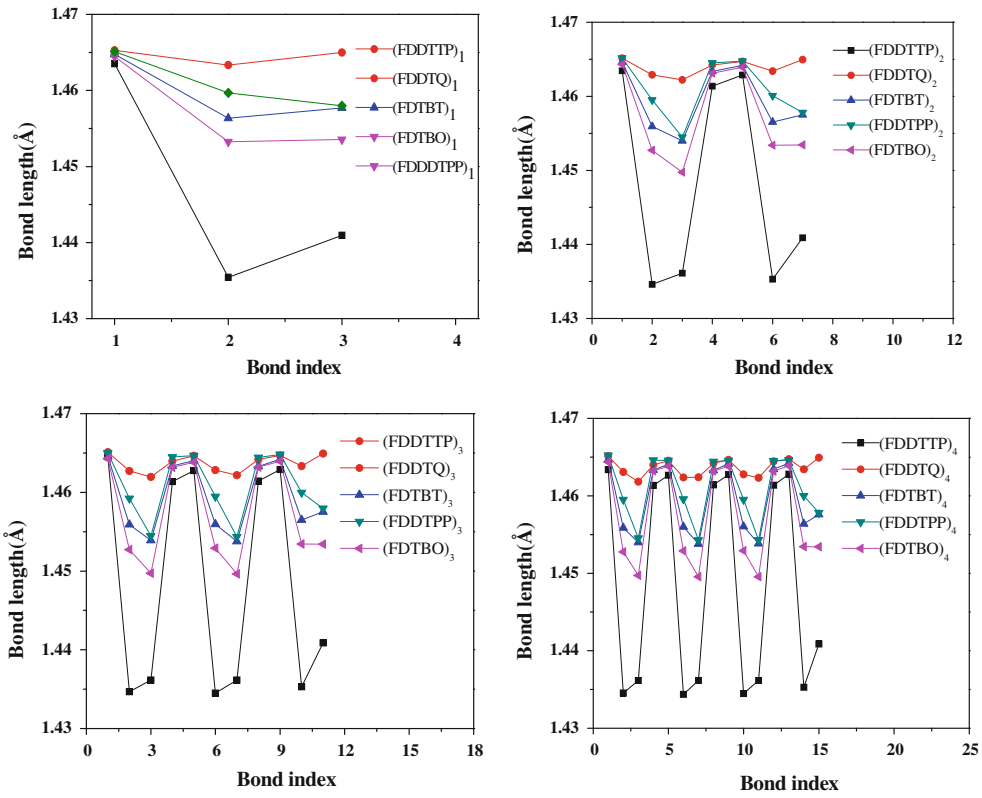

Fig. 2 C–C bond length alternation pattern for $(FDDTQ)_n$, $(FDTBT)_n$, $(FDDTTP)_n$, $(FDDTPP)_n$, and $(FDTBO)_n$. ($n = 1$–4), the bond index in each repeat unit are labeled in Fig. 1

Table 1 Selected important dihedral angles (°) of $(FDDTQ)_n$, $(FDTBT)_n$, $(FDDTTP)_n$, $(FDDTPP)_n$, and $(FDTBO)_n$

$(FDDTTP)_n$					$(FDDTQ)_n$				
	$n = 1$	$n = 2$	$n = 3$	$n = 4$		$n = 1$	$n = 2$	$n = 3$	$n = 4$
F-T	24.1	24.4	24.6	24.3	F-T	153.4	154.1	153.5	154.9
T-TP	179.1	178.7	179.1	179.7	T-Q	11.5	4.5	8.9	4.4
TP-T	0.1	1	0.9	0.3	Q-T	168.6	172.6	171.4	170.7
T-F		156.6	156.6	156.1	T-F		25.3	27.3	25.2
F-T		23.6	22.7	23.6	F-T		154.4	153.6	154
T-TP		178.8	179.2	179.6	T-Q		4.9	9.6	3.2
TP-T		0	0.4	0.2	Q-T		171.2	171.7	169.5
T-F			157.7	155.7	T-F			25.7	27.1
F-T			23.7	23.4	F-T			154.6	153.4
T-TP			179.5	179.4	T-Q			5.1	4.4
TP-T			0.1	1.7	Q-T			171.4	170.8
T-F				159.1	T-F				25.2
F-T				23.3	F-T				153.2
T-TP				179.2	T-Q				4.4
TP-T				0	Q-T				168.4
$(FDTBT)_n$					$(FDDTPP)_n$				
	$n = 1$	$n = 2$	$n = 3$	$n = 4$		$n = 1$	$n = 2$	$n = 3$	$n = 4$
F-T	155.6	155.2	154.8	155	F-T	154.4	154.5	154.1	153.9
T-BT	7.4	4.6	5.3	4.9	T-PP	11.3	170.8	12.8	169.4
BT-T	0.1	4.9	173.8	5.4	PP-T	179.8	179.9	1.6	179.4
T-F		156.6	157.2	156.2	T-F		25.1	26.8	24.1
F-T		155.9	156.2	156.1	F-T		154.6	156.7	153.0
T-BT		6.8	5.5	2.3	T-PP		168.1	8.3	169.9
BT-T		1.2	172.8	4.4	PP-T		179.8	0.6	179.6
T-F			156.4	154.7	T-F			25.5	23.7
F-T			156.6	156.3	F-T			155.0	153.5
T-BT			7.8	6.3	T-PP			10.9	169.1
BT-T			177.3	4.6	PP-T			0.2	179.7
T-F				155.9	T-F				24.4
F-T				156.4	F-T				154.1
T-BT				6.9	T-PP				172.1
BT-T				4.0	PP-T				179.9

$(FDTBO)_n$				
	$n = 1$	$n = 2$	$n = 3$	$n = 4$
F-T	23.8	24.8	25.7	24.7
T-BO	176.4	177.8	178.7	177.0
BO-T	179.9	178	177.2	177.3
T-F		24.9	24.8	24.3
F-T		24.8	24.5	23.3
T-BO		177.7	177.3	176.9
BO-T		180	177.7	177.8
T-F			24	24.1
F-T			24.8	24.0
T-BO			179.9	178.6
BO-T				177.9

Table 1 continued

$(FDTBO)_n$				
	$n = 1$	$n = 2$	$n = 3$	$n = 4$
T-F				25.4
F-T				24.6
T-BO				177.5
BO-T				178.9

F, T, Q, BT, TP, BO, and PP refer to 2,7-(9,9′-dihexylfluorene), thiophene, quinoxaline, 2,1,3-benzothiadiazole, thieno[3,4-b]pyrazine, 2,1,3-benzooxadiazole, and pyridopyrazine, respectively

Table 2 Maximum (Δd_{max}), averaged (Δd_{av}), and total ($\Sigma\Delta d_i$) changes in the lengths of the C–C bonds along the molecular backbone from the neutral state to the radical cation/anion state for $(FDDTQ)_n$, $(FDTBT)_n$, $(FDDTTP)_n$, $(FDDTPP)_n$, and $(FDTBO)_n$

	$n = 1$	$n = 2$	$n = 3$	$n = 4$
$(FDDTTP)_n$				
Δd_{max} (Å)	0.023/0.024	0.020/0.014	0.012/0.009	0.009/0.007
Δd_{av} (Å)	0.026/0.019	0.014/0.010	0.009/0.006	0.007/0.005
$\Sigma\Delta d_i$ (Å)	0.079/0.057	0.100/0.070	0.103/0.072	0.105/0.070
$(FDDTQ)_n$				
Δd_{max} (Å)	0.030/0.026	0.018/0.014	0.012/0.009	0.009/0.006
Δd_{av} (Å)	0.026/0.019	0.014/0.010	0.009/0.007	0.007/0.005
$\Sigma\Delta d_i$ (Å)	0.079/0.058	0.096/0.070	0.096/0.072	0.098/0.070
$(FDTBT)_n$				
Δd_{max} (Å)	0.029/0.019	0.019/0.010	0.013/0.006	0.009/0.004
Δd_{av} (Å)	0.027/0.015	0.015/0.007	0.009/0.005	0.007/0.003
$\Sigma\Delta d_i$ (Å)	0.080/0.046	0.099/0.050	0.093/0.048	0.095/0.046
$(FDTBO)_n$				
Δd_{max} (Å)	0.029/0.021	0.020/0.012	0.013/0.007	0.010/0.005
Δd_{av} (Å)	0.026/0.017	0.014/0.008	0.009/0.005	0.007/0.003
$\Sigma\Delta d_i$ (Å)	0.079/0.050	0.099/0.057	0.100/0.057	0.100/0.058
$(FDDTPP)_n$				
Δd_{max} (Å)	0.029/0.02	0.018/0.012	0.011/0.008	0.008/0.006
Δd_{av} (Å)	0.027/0.046	0.014/0.008	0.011/0.005	0.006/0.004
$\Sigma\Delta d_i$ (Å)	0.081/0.015	0.096/0.054	0.100/0.054	0.101/0.054

is typically expected for chain-end effects. Figure 3 also shows that the localized properties of HOMOs and LUMOs have small change with the increasing unit number. The HOMO delocalized the middle part of π-conjugated backbone, and the LUMO are localized on the donor and acceptor units, which indicates that the donor and acceptor units play important effect on the HOMO and LUMO of the copolymers.

The HOMO and LUMO energies in experiments were calculated from one empirical formula proposed by Brédas [40] based on the onset of the oxidation and reduction peaks measured by cyclic voltammetry, assuming the absolute energy level of ferrocene/ferrocenium to be

Table 3 The HOMO and LUMO energies, HOMO–LUMO gaps (ΔE), and the singlet lowest excitation energies (E_g) (in eV) of $(FDDTQ)_n$, $(FDTBT)_n$, $(FDDTTP)_n$, $(FDDTPP)_n$, and $(FDTBO)_n$ (n = 1–4, ∞) and comparison with experimental data

Oligomer	$n = 1$	$n = 2$	$n = 3$	$n = 4$	$n = \infty$	Exp[a]
$(FDDTTP)_n$						
$-E_{HOMO}$	4.71	4.57	4.52	4.51	4.43	4.97
$-E_{LUMO}$	2.43	2.51	2.55	2.56	2.60	3.76
ΔE	2.28	2.06	1.96	1.95	1.82	1.21
E_g (TD)	2.03	1.79	1.70	1.66	1.53	1.68
$(FDDTQ)_n$						
$-E_{HOMO}$	4.93	4.74	4.69	4.67	4.58	5.03
$-E_{LUMO}$	2.14	2.24	2.27	2.28	2.33	3.23
ΔE	2.79	2.50	2.42	2.38	2.23	1.80
E_g (TD)	2.45	2.16	2.08	2.05	1.90	1.94
$(FDTBT)_n$						
$-E_{HOMO}$	5.09	4.93	4.89	4.88	4.79	5.06
$-E_{LUMO}$	2.61	2.68	2.71	2.72	2.75	3.29
ΔE	2.48	2.25	2.18	2.15	2.03	1.77
E_g (TD)	2.15	1.93	1.86	1.81	1.70	1.82
$(FDDTPP)_n$						
$-E_{HOMO}$	5.02	4.84	4.79	4.78	4.68	–
$-E_{LUMO}$	2.36	2.44	2.48	2.49	2.53	–
ΔE	2.66	2.39	2.31	2.29	2.14	–
E_g (TD)	2.32	2.05	1.97	1.93	1.79	–
$(FDTBO)_n$						
$-E_{HOMO}$	5.22	5.07	5.03	5.02	4.94	–
$-E_{LUMO}$	2.68	2.77	2.82	2.84	2.88	–
ΔE	2.54	2.29	2.21	2.18	2.05	–
E_g (TD)	2.27	2.00	1.91	1.87	1.73	–

[a] The data are measured in film in ref [15, 42]

4.8 eV below vacuum. The preliminary hole/electron injection properties of the materials are usually estimated by the values of HOMO and LUMO in accord with the work function values of cathode and anode. The hole transport materials with the smaller negative value of HOMO can lose their electrons more easily, while the electron transport materials with larger negative value of

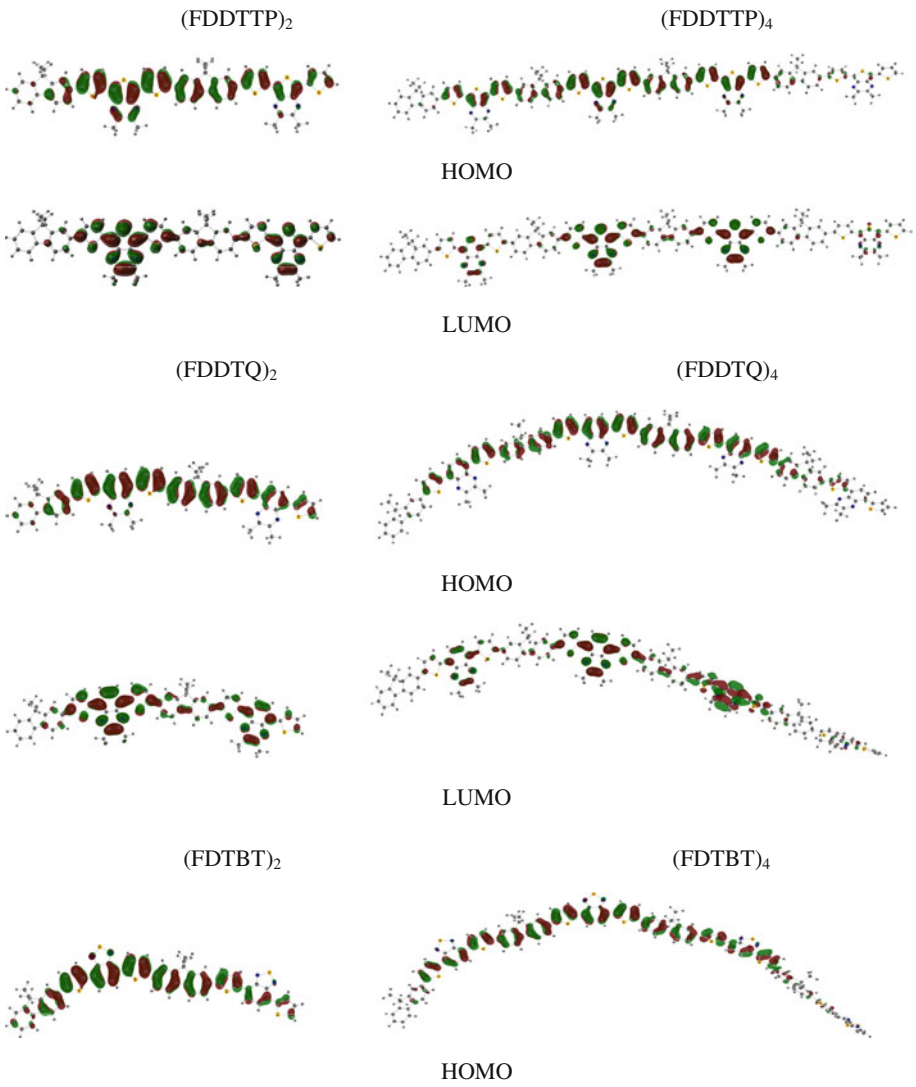

Fig. 3 The contour plots of HOMO and LUMO orbitals of $(FDDTQ)_n$, $(FDTBT)_n$, $(FDDTTP)_n$, $(FDDTPP)_n$, and $(FDTBO)_n$ ($n = 2,4$)

LUMO can accept electrons more easily. The HOMO and LUMO energies were further calculated by DFT method in this work. In order to more easily and vividly observe the variations in the HOMOs, LUMOs, and energy gaps, the frontier molecular orbitals (MO) energies and corresponding density of state (DOS) [41] of each oligomer are shown in Fig. 4. The negative energies of HOMO and LUMO are listed in Table 3, together with the HOMO–LUMO gaps, singlet lowest excitation energies, and available experimental data.

Table 3 and Fig. 4 show that the HOMO and LUMO energies have the same trend that with the increasing conjugation lengths, the HOMO energies increase, whereas the LUMO energies decrease. Table 3 and Fig. 4 also show that the calculated HOMO energies of the five series gradually close to the experimental values with increasing the values of *n*. The negative energies of HOMO increase in the sequence of PFDDTBO > PFDTBT > PFDDTPP > PFDDTQ > PFDDTTP, which exhibits that the copolymer with **TP** possesses better hole injection properties than others with **Q** or **PP** or **BT** or **BO**. The sequence of negative LUMO energies of the copolymers is in the sequence of PFDDTQ < PFDDTPP < PFDDTTP < PFDTBT < PFDTBO, which is in good agreement with the experimental sequence of PFDDTQ, PFDTBT, PFDDTTP. There are some changes in energies of LUMO with the experimental results because the theoretical calculations do not consider the polarization effects and intermolecular packing forces. This approach can be expected to be used to provide valuable information on estimating band gaps of polymers and oligomers.

For observing the variations in HOMOs, LUMOs, and energy gaps, the sets of one-electron energy levels of all oligomers (from HOMO−3 to LUMO+3) are plotted in Fig. 5. Take $(FDDTTP)_4$ (0.09, 0.04 eV) as an example, the energy difference between HOMO and HOMO−1 and LUMO and LUMO+1 is very small. This suggests that it is possible for the promotion of an electron from HOMO−1

Fig. 3 continued

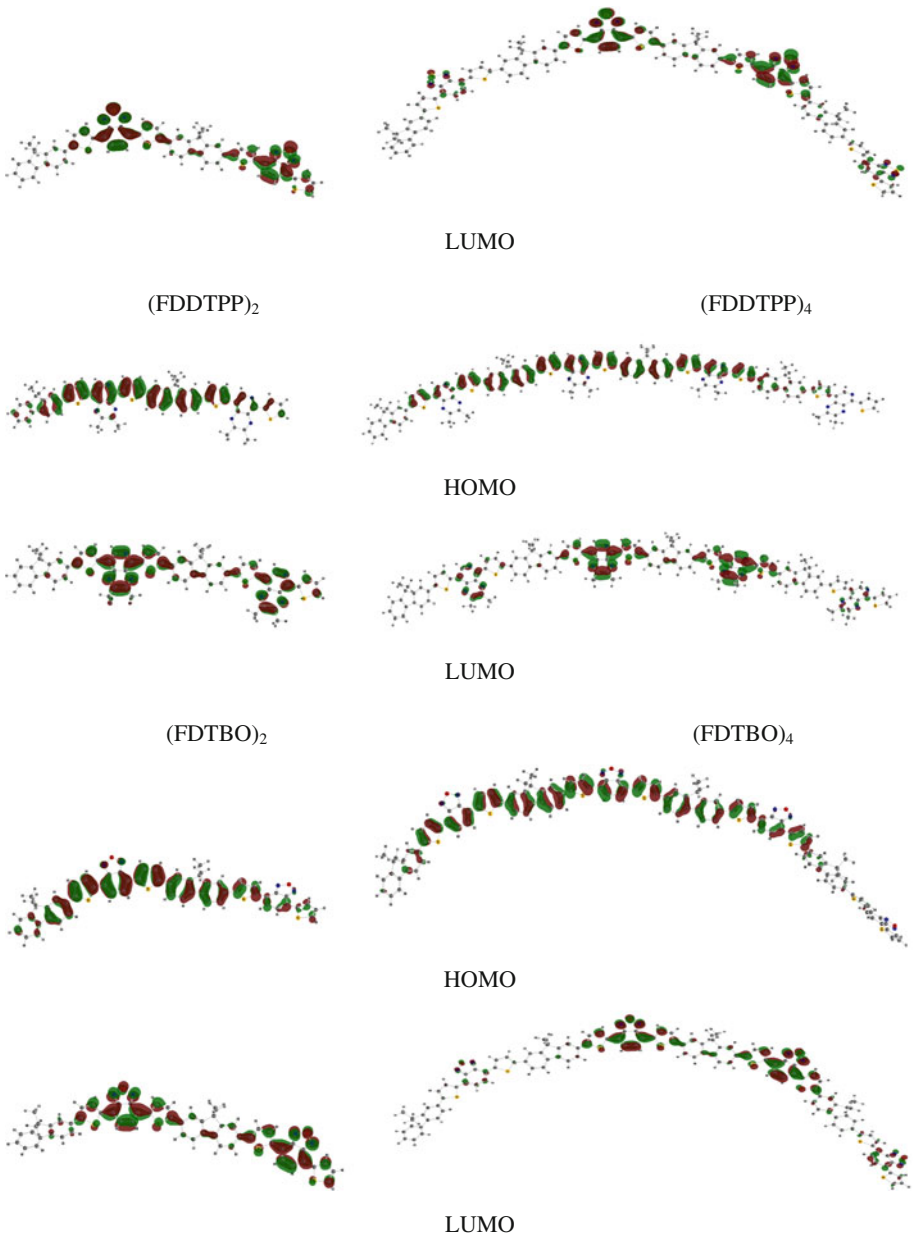

to LUMO, HOMO to LUMO+1, or HOMO−1 to LUMO+1, which will be further testified in Sects. 3.4 and 3.5.

The relationships between the calculated ΔE, E_g, HOMO, LUMO, and the inverse chain length are plotted in Fig. 6. Figure 6 describes the evolution of the calculated HOMO and LUMO energies as a function of the inverse number of monomer units in $(FDDTQ)_n$, $(FDTBT)_n$, $(FDDTTP)_n$, $(FDDTPP)_n$, and $(FDTBO)_n$ ($n = 1$–4). It is usual in π-conjugated systems that the energies of the frontier electronic levels evolve linearly with inverse chain lengths in the five systems. The HOMO energies will increase, whereas the LUMO energies will decrease with increasing conjugation lengths according to above relationship [43].

As shown in Table 3 and Fig. 6, the HOMO–LUMO gaps and the singlet lowest excitation energies in $(FDDTQ)_n$, $(FDTBT)_n$, $(FDDTTP)_n$, $(FDDTPP)_n$, and $(FDTBO)_n$ ($n = 1$–4) are narrowed gradually, which indicates that it is easier to promote an electron from HOMO to LUMO with increasing the values of n. Obviously, the sequences of E_g and HOMO–LUMO gap presented in Table 3 exist good agreements with the experimental sequences. The E_g and HOMO–LUMO gap of PFDTBT are smaller than PFDDTP. The reason may be that **BT** moiety with a six-membered ring has a larger torsional angle than **TP** segment with a five-membered ring and results in the reduction in the π-conjugation. It also indicates that the backbone planarity and the degree of ICT for

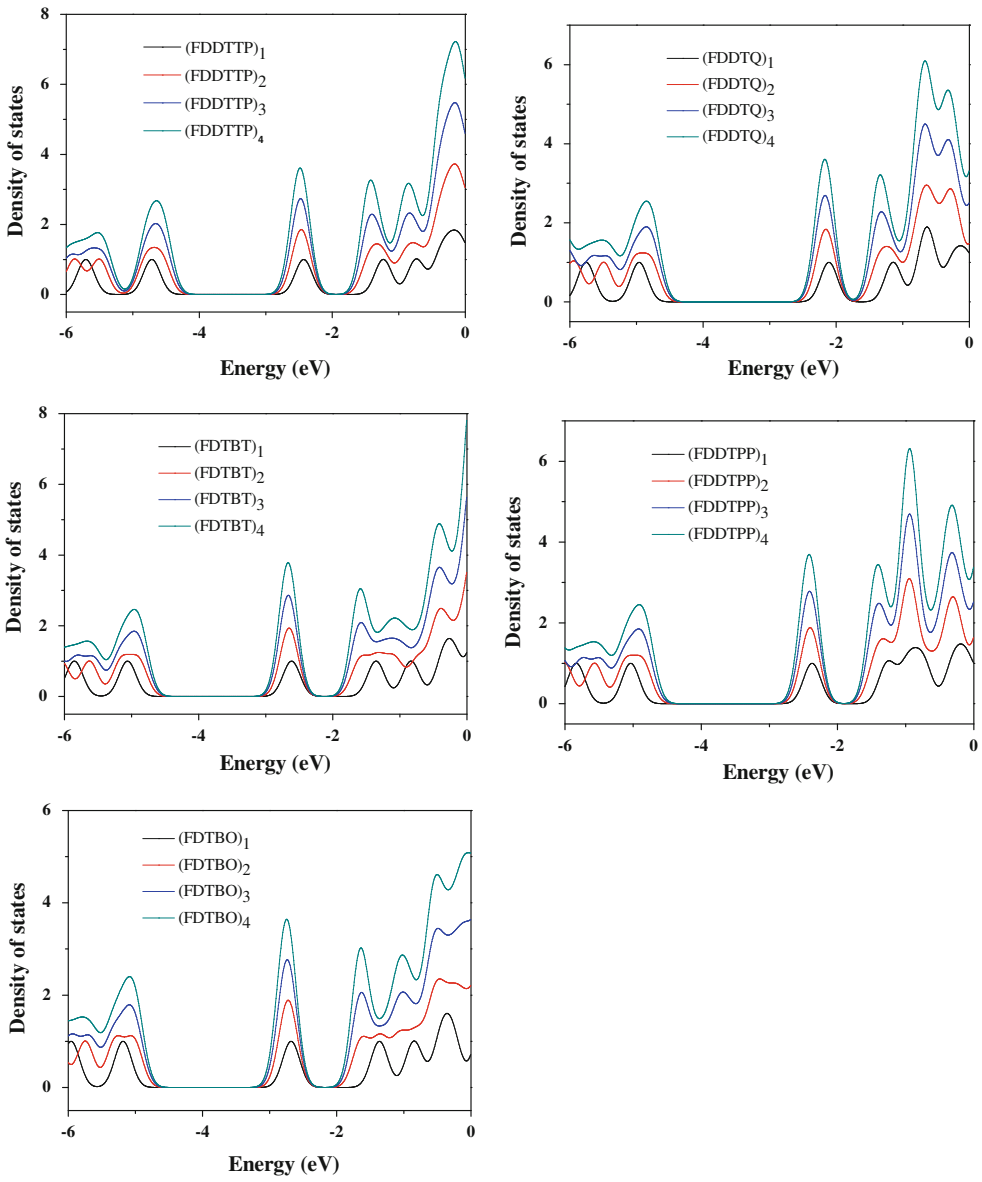

Fig. 4 The density of states spectrum of each oligomer

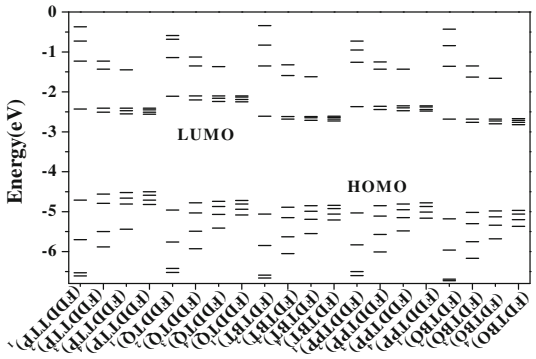

Fig. 5 Sets of one-electron energy levels of each oligomer

TP-thiophene are probably higher than those of **BT-**thiophene system. However, there is still some difference between the calculated results and the experimental values. This discrepancy is in part due to the relatively large size of the studied systems and the reciprocal dependence of the energy gap on the number of repeat units. Another factor responsible for deviations from experimental is that the predicted band gaps are obtained in the isolated gas phase, while the experimental band gaps are measured in thin films by cyclic voltammetry where the solid-state packing effects were involved.

3.3 Ionization potentials and electron affinities

The adequate and balanced transport of both injected electrons and holes are important in optimizing the device performance of donor–acceptor conjugated copolymers. The ionization potential (IP) and electron affinity (EA) are well-defined properties that can be calculated by DFT to

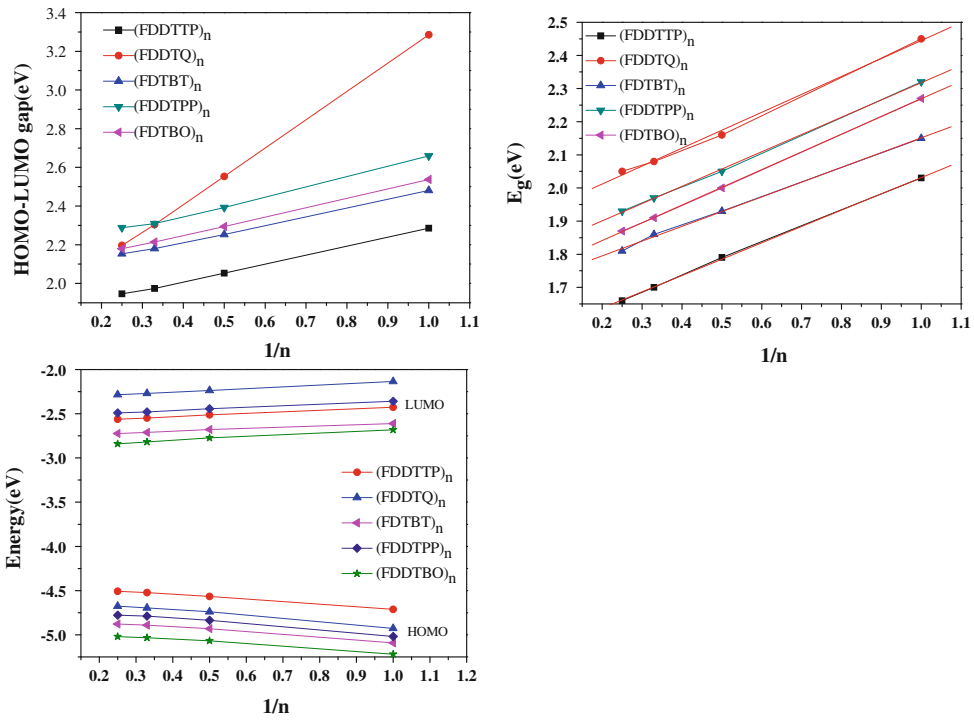

Fig. 6 HOMO and LUMO energies, HOMO-LUMO gaps by B3LYP, and the lowest excitation energies E_g's of the five series by TD-DFT as a function of reciprocal chain length n in oligomers

estimate the energy barriers for the injection of carriers into the polymer active layer. The calculated IPs(v, a), EAs(v, a), and extraction potentials (including HEP and EEP for the hole and electron) are listed in Table 4. The IPs, EAs, HEPs, and EEPs for infinite chains of the polymers were determined by plotting these values of oligomers against the reciprocal of the number of modeling polymeric units and by extrapolating the number of units to infinity.

For the application of polymers in organic light-emitting devices, one general challenge is to achieve high EA values for improving electron injection/transport and low IP values for better hole injection/transport. Table 4 shows that the values of the Ips (v, a) progressively decrease, while the Eas (v, a) turn high gradually from $n = 1$ to 4. For PFDDTTP, PFDDTQ, PFDTBT, PFDDTPP, and PFDTBO, the vertical and adiabatic energies required to create a hole in each polymer are around 4.7, 4.9, 5.0, 5.0, and 5.2 eV, respectively, implying the hole-creating ability of these five polymers decreasing in the sequence of PFDDTTP < PFDDTQ < PFDDTPP < PFDTBT < PFDTBO. Because of the lower IP value of the hole-transporting materials, it is easier to enter the holes from the hole transport layer to the emitter layer. This sequence is consistent with the analysis for HOMO energies. Thus, the hole injection and transportation of PFDDTTP and PFDDTQ are expected to be easier than PFDTBT, PFDDTPP, and PFDTBO. The extraction of an electron from the anion requires about 2.34, 2.34, and 2.37 eV by three methods for PFDDTTP, respectively. And the extraction of an electron from the anion requires about 2.0, 2.5, 2.2, and 2.6 eV for PFDDTQ, PFDTBT, PFDDTPP, and PFDTBO, respectively. The change trends of $EA_{(a)}$ are similar to those of the negative of LUMO energies. Because of the higher EA value of the electron-transporting materials, it is easier to inject electrons from cathode. This indicates that the combination with electron-withdrawing **BO** and **BT** will improve the electron transport properties of the copolymers. It is concluded that the optoelectronic properties of a conjugated polymer are primarily governed by the chemical structure of the polymer backbone.

3.4 Absorption spectra

The detailed electronic transitions, including the maximum absorption wavelength (λ), the largest oscillator strength (f), and the configurations for the main and $S_0 \rightarrow S_1$ electronic transitions of $(FDDTQ)_n$, $(FDTBT)_n$, $(FDDTTP)_n$, $(FDDTPP)_n$, and $(FDTBO)_n$ ($n = 1$–4) are summarized in Table 5. The simulated Gaussian type absorption spectra of $(FDDTQ)_4$, $(FDTBT)_4$, $(FDDTTP)_4$, $(FDDTPP)_4$, and $(FDTBO)_4$ are shown in Fig. 7. The lowest-lying absorption excitation energy of $(FDDTQ)_n$, $(FDTBT)_n$, $(FDDTTP)_n$, $(FDDTPP)_n$, and $(FDTBO)_n$ ($n = 1$–4, ∞) obtained by extrapolation method is also shown in Fig. 7 and Table 3.

As shown in Table 5, some interesting trends are observed in these oligomers. All electronic transitions are of $\pi \rightarrow \pi^*$ type in the calculated singlet–singlet transitions. The detailed configurations for the transition also

Table 4 Ionization potentials, electron affinities, and extraction potentials for each oligomer (in eV)

Oligomer	IP(a)	IP(v)	HEP	EA(v)	EA(a)	EEP
$(FDDTTP)_n$						
$n = 1$	5.68	5.83	5.68	1.23	1.37	1.37
$n = 2$	5.22	5.31	5.21	1.76	1.83	1.83
$n = 3$	5.04	5.11	5.04	1.96	2.01	2.02
$n = 4$	4.94	4.98	4.90	2.09	2.12	2.16
$n = \infty$	4.71	4.73	4.68	2.34	2.34	2.37
$(FDDTQ)_n$						
$n = 1$	5.89	6.06	5.75	0.92	1.09	1.22
$n = 2$	5.43	5.54	5.34	1.45	1.55	1.62
$n = 3$	5.26	5.35	5.19	1.66	1.73	1.79
$n = 4$	5.14	5.21	5.06	1.77	1.85	1.90
$n = \infty$	4.92	4.97	4.87	2.03	2.07	2.09
$(FDTBT)_n$						
$n = 1$	6.02	6.17	5.88	1.31	1.44	1.56
$n = 2$	5.55	5.65	5.46	1.88	1.95	2.00
$n = 3$	5.38	5.45	5.32	2.10	2.15	2.19
$n = 4$	5.28	5.33	5.23	2.22	2.26	2.29
$n = \infty$	5.05	5.08	5.03	2.50	2.51	2.51
$(FDDTPP)_n$						
$n = 1$	5.97	6.21	5.84	1.15	1.30	1.42
$n = 2$	5.50	5.61	5.40	1.68	1.76	1.82
$n = 3$	5.32	5.39	5.26	1.89	1.94	1.99
$n = 4$	5.22	5.31	5.17	2.01	2.04	2.12
$n = \infty$	4.99	5.00	4.96	2.26	2.27	2.30
$(FDTBO)_n$						
$n = 1$	6.15	6.30	6.02	1.38	1.52	1.63
$n = 2$	5.69	5.79	5.59	1.96	2.03	2.10
$n = 3$	5.51	5.58	5.45	2.19	2.24	2.28
$n = 4$	5.41	5.46	5.36	2.32	2.35	2.40
$n = \infty$	5.18	5.21	5.15	2.60	2.60	2.62

show that HOMO → LUMO transition mainly dominates the transition. The strongest absorption peaks with largest oscillator strengths for these oligomers arise from $S_0 \rightarrow S_1$, which is mainly attributed to the promotion of an electron from HOMO to LUMO. In the case of the oscillator strength, the absorption wavelengths arising from $S_0 \rightarrow S_1$ increase progressively with enlarging the conjugation lengths. Since HOMO → LUMO transition is predominant in $S_0 \rightarrow S_1$, the HOMO–LUMO gaps will decrease with the extending molecular size. The absorption spectrum of S_1 also exhibits red-shift with increasing the conjugation lengths.

Take $(FDDTTP)_n$ ($n = 1$–4) as an example, the lowest optically allowed electronic transition ($\pi \rightarrow \pi^*$) are $S_0 \rightarrow S_1$ with the strongest oscillator strengths (f). As listed in Table 5, the absorption spectra of S_1 are 610, 693, 730, and 749 nm for $(FDDTTP)_1$, $(FDDTTP)_2$, $(FDDTTP)_3$, and $(FDDTTP)_4$, respectively. It is obvious that the absorption spectrum of S_1 exhibits red-shift, and the oscillator strength increases with enlarging the conjugation lengths. The detailed configurations for the transition also show that HOMO → LUMO transition mainly dominates the transition. As shown in Fig. 7, $(FDDTTP)_4$ has only one absorption peak at 749 nm. From Table 5, we found that the TD-DFT results deviate from the observed experimental absorption spectra ($n = \infty$). The reason is attributed to the conjugation lengths, different mediums, drawbacks of TD-DFT itself, and so on. As we know, TD-DFT method is a good predictive tool for absorption spectra of small molecules. However, it has some defects to study the largely extended systems. Because it is not infrequent that the optical properties reach saturation already for quite short chain length, whereas the orbital energies still continue to change for longer oligomers. The exchange–correlation functionals decrease with the increase in chain length. The trend is the well-known in line with the expectation that the electronic repulsion is smaller in more extended systems [38, 44, 45]. However, the TD-DFT results could still be reasonable to predict the variation trends because the atomic structures of the molecules and copolymers are alike and calculated with the same methods and basis sets.

3.5 Properties of excited-state structures and emission spectra

The calculation of excited-state geometries (S_1) and ground states (S_0) of the monomers are optimized by TD-DFT/6-31G(d) method. Comparison of S_1 with S_0 of $(FDDTQ)_1$, $(FDTBT)_1$, $(FDDTTP)_1$, $(FDDTPP)_1$, and $(FDTBO)_1$ is described in Fig. 8. The bond length alternation (BLA) and inter-ring dihedral angles are listed in Table 6 when excited from ground to excited states.

Bond length alternation (BLA) [46] is the bond length difference between single and double carbon–carbon bonds, which represents a major contribution to the existence of a finite band gap in conjugated oligomers and polymers. In the five structures of the model oligomers, it might be feasible to investigate the BLA of the invariable thiophene between fluorene and acceptors, which is defined as δ. Taking oligomer $(FDDTTP)_1$ as an example, δ is calculated as the difference between the bond length C_3–C_4 (1.411 Å) and the average bond length of $C_4 = C_5$ (1.381 Å) and $C_2 = C_3$ (1.386 Å; shown in Table 6). Since the thiophene donor is the same for the five oligomers, the δ of $(FDDTTP)_1$ is the smallest in the five oligomers, which also giving rise to the smallest band gap. This result indicates that the bond length alternation plays a major role in band gap reduction for oligomers. As shown in Fig. 8,

Table 5 Electronic transition data obtained by the TD-DFT//B3LYP/6-31G

System	Electronic transitions	λ (nm)	λ_{exp} (nm)[a]	f	Main configurations
$(FDDTTP)_1$	$S_0 \rightarrow S_1$	610		0.61	H → L (98%)
$(FDDTTP)_2$	$S_0 \rightarrow S_1$	693		1.91	H → L (81%)
$(FDDTTP)_3$	$S_0 \rightarrow S_1$	730		2.46	H → L (89%)
$(FDDTTP)_4$	$S_0 \rightarrow S_1$	749		3.43	H → L (78%)
$(FDDTTP)_\infty$			416, 616		
$(FDDTQ)_1$	$S_0 \rightarrow S_1$	504		0.74	H → L (98%)
$(FDDTQ)_2$	$S_0 \rightarrow S_1$	571		2.17	H → L (93%)
$(FDDTQ)_3$	$S_0 \rightarrow S_1$	594		3.47	H → L (85%)
$(FDDTQ)_4$	$S_0 \rightarrow S_1$	614		4.45	H → L (61%)
$(FDDTQ)_\infty$			374, 502		
$(FDTBT)_1$	$S_0 \rightarrow S_1$	575		0.58	H → L (83%)
$(FDTBT)_2$	$S_0 \rightarrow S_1$	639		1.66	H → L (87%)
$(FDTBT)_3$	$S_0 \rightarrow S_1$	666		2.47	H → L (81%)
$(FDTBT)_4$	$S_0 \rightarrow S_1$	685		3.65	H → L (79%)
$(FDTBT)_\infty$			406, 576		
$(FDDTPP)_1$	$S_0 \rightarrow S_1$	532		0.63	H → L (98%)
$(FDDTPP)_2$	$S_0 \rightarrow S_1$	595		1.96	H → L (68%)
$(FDDTPP)_3$	$S_0 \rightarrow S_1$	626		3.24	H → L (85%)
$(FDDTPP)_4$	$S_0 \rightarrow S_1$	635		4.43	H → L (79%)
$(FDDTPP)_\infty$			–		
$(FDTBO)_1$	$S_0 \rightarrow S_1$	545		0.83	H → L (99%)
$(FDTBO)_2$	$S_0 \rightarrow S_1$	617		2.18	H → L (90%)
$(FDTBO)_3$	$S_0 \rightarrow S_1$	647		3.14	H → L (82%)
$(FDTBO)_4$	$S_0 \rightarrow S_1$	661		3.90	H → L (71%)
$(FDTBO)_\infty$			–		

H HOMO, *L* LUMO

[a] The data are measured in film in ref [15, 42]

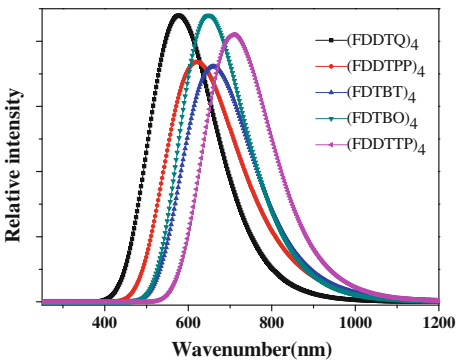

Fig. 7 The Gaussian type absorption spectra for $(FDDTQ)_4$, $(FDTBT)_4$, $(FDDTTP)_4$, $(FDDTPP)_4$, and $(FDTBO)_4$

the bond length of C_1–C_{13} (1.529 Å) in $(FDDTTP)_1$ and those of C_4–C_7 (1.529 Å) in other four oligomers are a little larger than the bond length of C_3–C_{11} (1.521 Å) in 2,7-di(2-thienyl)-9,9-dihexylfluorene [47]. However, the bond length of C_1–C_{13} (1.529 Å) in $(FDDTTP)_1$ is the same as that of C_9–C_{10} (1.529 Å) in 2,7-dibromo-9,9-octylfluorene [48] The bond length of C_1–C_{22} (1.410 Å) in $(FDDTTP)_1$ and the bond lengths of C_4–C_5 (1.410 Å) in other four oligomers are larger than the bond length of C_3–C_4 (1.402 Å) in 2,7-di(2-thienyl)-9,9-dihexylfluorene [47]. The φ_2 and φ_3 in $(FDDTQ)_1$ are 11.5° and 168.6°, respectively, indicating that the donor–acceptor–donor in $(FDDTQ)_1$ is a nearly planar conformation. This is the same as the conformation reported in previous literature [49]. But the φ_3 in $(FDDTTP)_1$ is smaller than the dihedral angle reported in the literature [49].

Figure 8 also shows that some bond lengths become longer after being excited, while some become shorter in $(FDDTQ)_1$, $(FDTBT)_1$, $(FDDTTP)_1$, $(FDDTPP)_1$, and $(FDTBO)_1$. Since the singlet state is related to an excitation from HOMO to LUMO in oligomers, we can investigate the bond length variation by just analyzing their HOMOs and LUMOs. Take $(FDDTTP)_1$ as an example, the HOMO is bonding across the r(25,27), r(17,15), r(1,22), r(10,22), r(9,6), r(6,7), r(6,7), r(4,5), r(2,3), r(11,24), r(20,27), r(28,29), and r(30,31), while the LUMO has nodes in these regions. The bond lengths possessing bonding character

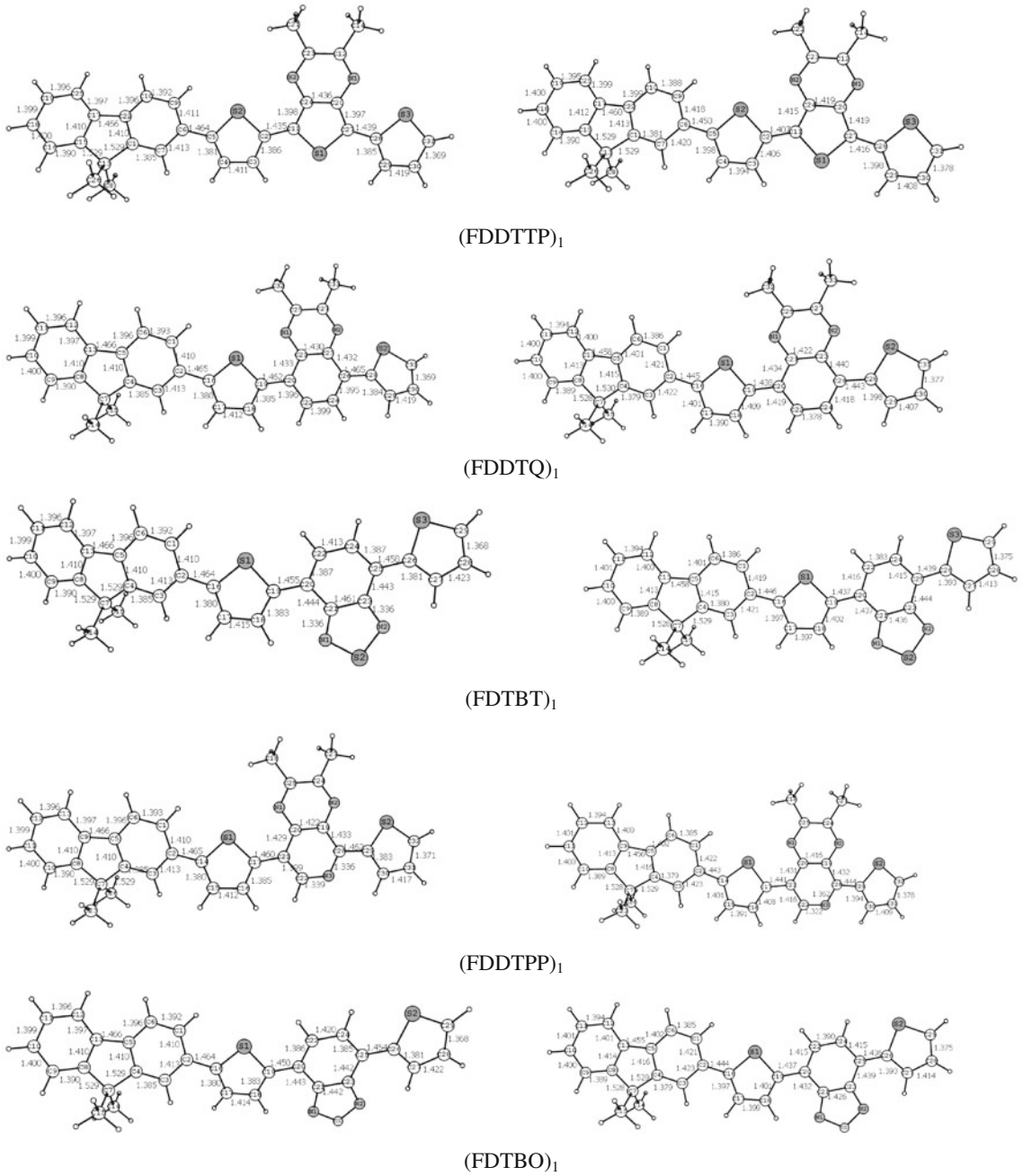

Fig. 8 Comparison of the excited structure (S_1) with the ground geometry (S_0) of $(FDDTQ)_1$, $(FDTBT)_1$, $(FDDTTP)_1$, $(FDDTPP)_1$, and $(FDTBO)_1$

(HOMO) and antibonding character (LUMO) will be lengthened upon excitation. This also can be seen from the bond lengths in $(FDDTQ)_1$, $(FDTBT)_1$, $(FDDTTP)_1$, $(FDDTPP)_1$, and $(FDTBO)_1$. The bridge bonds between each conjugation segment rotate to some extent when the molecule is excited from ground to excited states. It can be seen that the dihedral angles φ_1 and φ_3 of $(FDDTTP)_1$ decrease from 24.1° and 0.1° to 8.4° and 0°. However, the dihedral angle φ_2 increases from 179.1° to 179.6°. As shown in Table 6, it is also obvious that the excited structures in these oligomers have a strong coplanar tendency. This indicates that the singlet excited state involving mainly the promotion of an electron from the HOMO to the LUMO will be more planar.

Based on the excited-state geometries optimized by TD-DFT/6-31G(d), the emission wavelengths of the monomers

are also computed by TD-DFT. The transition characters are listed in Table 7, and the simulated Gaussian type emission spectra of $(FDDTQ)_1$, $(FDTBT)_1$, $(FDDTTP)_1$, $(FDDTPP)_1$, and $(FDTBO)_1$ are shown in Fig. 9.

As shown in Table 7 and Fig. 9, the emission peaks with strongest oscillator strength are all assigned to $\pi \rightarrow \pi^*$ character arising from S_1 to S_0. However, it is easy to see that the areas of emission curves are larger than those from absorption spectra because the torsion angles between acceptor and donor have obvious changes leading to great variation in vertical transition energies. The emission wavelengths also show some bathochromic shifts compared to the absorption spectra, which consists with the tendency of those obtained from experiments [42]. Through analyzing the transition configuration for the fluorescence, the calculated emission is just reverse process of the lowest-lying absorption because the emission and the lowest-lying absorptions have the same symmetries and transition characters.

4 Conclusion

The geometries, electronic structures, IPs, EAs, absorption, and fluorescence properties of five series oligomers $(FDDTQ)_n$, $(FDTBT)_n$, $(FDDTTP)_n$, $(FDDTPP)_n$, and $(FDTBO)_n$ ($n = 1$–4) in this work. The five series oligomers show smooth binomial relationship between inverse repeating unit numbers ($1/n$) and the HOMO–LUMO gaps, IPs, EAs, and the optical properties. The order of the band gaps is $(FDDTQ)_n > (FDDTBO)_n > (FDDTPP)_n > (FDTBT)_n > (FDDTTP)_n$, which is on the reverse trend of luminescence. The strong acceptor strength of **TP** unit and more coplanar backbone in $(PFDTTP)_n$ resulted in a high ICT and thus leading to the lowest band gap among the five copolymers. In addition, the discussion on the value of IP and EA indicates that the hole injection and transportation of $(PFDDTTP)_n$ and $(PFDDTQ)_n$ are expected to be easier than $(PFDTBT)_n$, $(PFDDTPP)_n$, and $(PFDTBO)_n$. Through analyzing the configuration of $(FDDTQ)_1$, $(FDTBT)_1$, $(FDDTTP)_1$, $(FDDTPP)_1$, and $(FDTBO)_1$ with different acceptors, the variations in bond lengths and inter-ring dihedral angles between acceptor and donor are given, which illuminates that the electronic effect of the acceptors will influence the molecular structure in the ground state and excited state. The present study suggested the importance of the acceptor structure on the electronic and optical properties of donor–acceptor conjugated copolymers.

Table 6 Selected inter-ring dihedral angles (deg) of $(FDDTQ)_1$, $(FDTBT)_1$, $(FDDTTP)_1$, $(FDDTPP)_1$, and $(FDTBO)_1$ in the ground and excited geometries, respectively, the dihedral angle index in each repeat unit are labeled in Fig. 1

Monomer	φ_1	φ_2	φ_3	δ
$(FDDTTP)_1$	24.1/8.4	179.1/179.6	0.1/0	0.028
$(FDDTQ)_1$	153.4/171.5	11.5/0.9	168.6/179.8	0.030
$(FDTBT)_1$	155.6/179.9	7.4/0	0.1/0	0.034
$(FDDTPP)_1$	154.4/179.9	11.3/0	179.8/180	0.030
$(FDTBO)_1$	24.7/0	176.2/180	179.9/180	0.033

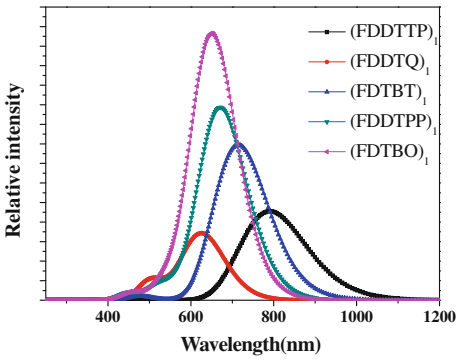

Fig. 9 The Gaussian type emission spectra of $(FDDTQ)_1$, $(FDTBT)_1$, $(FDDTTP)_1$, $(FDDTPP)_1$, and $(FDTBO)_1$

Table 7 Emission spectra obtained by TD-DFT of $(FDDTQ)_1$, $(FDTBT)_1$, $(FDDTTP)_1$, $(FDDTPP)_1$, and $(FDTBO)_1$

System	Electronic transitions	λ (nm) (eV)	λ_{exp} (nm)[a]	f	Main configurations
$(FDDTTP)_1$	$S_0 \leftarrow S_1$	790 (1.57)	736	0.45	H → L (70%)
$(FDDTQ)_1$	$S_0 \leftarrow S_1$	623 (1.99)	620	0.62	H → L (69%)
$(FDTBT)_1$	$S_0 \leftarrow S_1$	714 (1.73)	677	0.45	H → L (70%)
$(FDDTPP)_1$	$S_0 \leftarrow S_1$	673 (1.84)	–	0.53	H → L (70%)
$(FDTBO)_1$	$S_0 \leftarrow S_1$	653 (1.89)	–	0.74	H → L (70%)

[a] The data are measured in film in ref [42]

Acknowledgments Financial supports from the NSFC (No. 20802033), NCET-10-0170, and KLEFCA-10HJYH03 are gratefully acknowledged.

References

1. Zotti G, Schiavon G, Zecchin S, Morin JF, Leclerc M (2002) Macromolecules 35:2122
2. Morin JF, Beaupré S, Leclerc M, Lévesque I, D'Iorio M (2002) Appl Phys Lett 80:341
3. Peng Q, Lu ZY, Huang Y, Xie MG, Han S-H, Peng JB, Cao Y (2004) Macromolecules 37:260
4. Babel A, Jenekhe SA (2003) J Am Chem Soc 125:13656
5. Kim JY, Lee K, Coates NE, Moses D, Nguyen TQ, Dante M, Heeger AJ (2007) Science 317:222
6. Senechal-David K, Hemeryck A, Tancrez N, Toupet L, Williams JA, Ledoux I, Zyss J, Boucekkine A, Guegan JP, Le BH, Maury O (2006) J Am Chem Soc 128:12243
7. Liu Y, Miao Q, Zhang SW, Huang X-B, Zheng L-F, Cheng YX (2008) Macromol Chem Phys 209:685
8. Yamamoto T, Zhou ZH, Kanbara T, Shimura M, Kizu K, Maruyama T, Nakamura Y, Fukuda T, Lee BL, Ooba N, Tomaru S, Kurihara T, Kaino T, Kubota K, Sasaki S (1996) J Am Chem Soc 118:10389
9. Akoudad S, Roncali J (1998) Chem Commun 19:2081
10. Tsai FC, Chang CC, Liu CL, Chen WC, Jenekhe SA (2005) Macromolecules 38:1958
11. Zhang X, Jenekhe SA (2000) Macromolecules 33:2069
12. Liu CC, Tsai FC, Chang CC, Hsieh KH, Lin JJ, Chen WC (2005) Polymer 46:4950
13. Liu J, Guo X, Bu LJ, Xie ZY, Cheng YX, Geng YH, Wang LX, Jing XB, Wang FS (2007) Adv Funct Mater 17:1917
14. Gadisa A, Mammo W, Andersson LM, Admassive S, Zhang F, Andersson MR, Inganäs O (2007) Adv Funct Mater 17:3836
15. Lee WY, Cheng KF, Wang TF, Chen WC, Tsai FY (2010) Thin Solid Films 518:2119
16. Hong SY, Song JMJ (1997) Chem Phys 107:10607
17. Moulé AJ, Tsami A, Bünnagel TW, Forster M, Kronenberg NM, Scharber M, Koppe M, Morana M, Brabec CJ, Meerholz K, Scherf U (2008) Chem Mater 20:4045
18. Baek NS, Hau SK, Yip HL, Acton O, Chen KS, Jen AKY (2008) Chem Mater 20:5734
19. Liu CL, Tsai JH, Lee WY, Chen WC, Jenekhe SA (2008) Macromolecules 41:6952
20. Babel A, Zhu Y, Cheng KF, Chen WC, Jenekhe SA (2007) Adv Funct Mater 17:2542
21. Soci C, Hwang IW, Moses D, Zhu Z, Waller D, Gaudiana R, Brabec CJ, Heeger AJ (2007) Adv Funct Mater 17:632
22. Horst W, Susanne S, Stefan J, Alexander VU, Axel HEM (2003) Macromolecules 36:3374
23. Yamamoto T, Fujiwara Y, Fukumoto H, Nakamura Y, Koshihara SY, Ishikawa T (2003) Polymer 44:4487
24. Ma J, Li SH, Jiang YS (2002) Macromolecules 35:1109
25. Liu LM, Wang XY, Wang YL, Peng XY, Mo YX (2009) J Polym Sci Part B Polym Phys 47:706
26. Frisch MJ, Trucks GW, Schlegel HB, Scuseria GE, Robb MA, Cheeseman JR, Scalmani G, Barone V, Mennucci B, Petersson GA, Nakatsuji H, Caricato M, Li X, Hratchian HP, Izmaylov AF, Bloino J, Zheng G, Sonnenberg JL, Hada M, Ehara M, Toyota K, Fukuda R, Hasegawa J, Ishida M, Nakajima T, Honda Y, Kitao O, Nakai H, Vreven T, Montgomery JJA, Peralta JE, Ogliaro F, Bearpark M, Heyd JJ, Brothers E, Kudin KN, Staroverov VN, Kobayashi R, Normand J, Raghavachari K, Rendell A, Burant JC, Iyengar SS, Tomasi J, Cossi M, Rega N, Millam JM, Klene M, Knox JE, Cross JB, Bakken V, Adamo C, Jaramillo J, Gomperts R, Stratmann RE, Yazyev O, Austin AJ, Cammi R, Pomelli C, Ochterski JW, Martin RL, Morokuma K, Zakrzewski VG, Voth GA, Salvador P, Dannenberg JJ, Dapprich S, Daniels AD, Farkas O, Foresman JB, Ortiz JV, Cioslowski J and Fox D J (2007) Gaussian 09, Revision A.02, Gaussian, Inc, Wallingford
27. Becke AD (1988) Phys Rev A 38:3098
28. Becke AD (1993) J Chem Phys 98:5648
29. Lee C, Yang W, Parr RG (1988) Phys Rev B 37:785
30. Hobza P, Sÿponer J (1999) Chem Rev 99:3247
31. Belletête M, Beaupré S, Bouchard J, Blondin P, Leclerc M, Durocher G (2000) J Phys Chem B 104:9118
32. Yang S, Olishevski P, Kertesz M (2004) Synth Met 141:171
33. Cao H, Ma J, Zhang GL, Jiang YS (2005) Macromolecules 8:1123
34. Zhou X, Ren AM, Feng JK (2004) Polymer 22:7747
35. Wang JF, Feng JK, Ren AM, Liu XD, Ma YG, Lu P, Zhang HX (2004) Macromolecules 37:3451
36. Casida ME, Jamorski C, Casida KC, Salahub DR (1998) J Chem Phys 108:4439
37. Duarte HA, Duani H, De Almeida WB (2003) Chem Phys Lett 369:114
38. Yang L, Feng JK, Ren AM (2005) J Org Chem 70:5987
39. Carrión S, Rodríguez-Ropero F, Aradilla D, Zanuy D, Casanovas J, Alemán C (2010) J Phys Chem B 114:3494
40. Brédas JL, Silbey R, Boudreaux DS, Chance RR (1983) J Am Chem Soc 105:6555
41. Ran XQ, Feng JK, Ren AM, Li WC, Zou LY, Sun CC (2009) J Phys Chem A 113:7933
42. Lee WY, Cheng KF, Wang TF, Chueh CC, Chen WC, Tuan CS, Lin JL (2007) Macromol Chem Phys 208:1919
43. Cornil J, Gueli I, Dkhissi A, Sancho-Garcia JC, Hennebicq E, Calbert JP, Lemaur V, Beljoone D, Brédas JLJ (2003) Chem Phys 18:6615
44. Grimme S, Parac M (2003) Chem Phys Chem 3:292
45. Ortiz RP, Delgado MCR, Casado J, Hernandez V, Kim OK, Woo HY, Navarrete LL (2004) J Am Chem Soc 126:13363
46. Kertesz M, Choi CH, Yang S (2005) Chem Rev 105:3448
47. Destri S, Pasini M, Botta C, Porzio M, Bertinia F, Marchiò L (2002) J Mater Chem 12:924
48. Leclerc M, Ranger M, Bélanger-Gariépy F (1998) Acta Cryst C54:799
49. Kitamura C, Tanaka S, Yamashita Y (1996) Chem Mater 8:570